International Journal of Computing and Digital Systems
ISSN (2210-142X)
Int. J. Com. Dig. Sys. 11, No.1 (Jan-2022)

https://dx.doi.org/10.12785/ijcds/110106

A Critical Review on Machine Learning based Liver Tumor Classification

Munipraveena Rela[1], Suryakari Nagaraja Rao[2] and Patil Ramana Reddy[3]

[1]*Department of Electronics and Communication Engineering, Jawaharlal Nehru Technological University Ananthapur, Ananthapuramu, A.P, India*

[2]*Department of Electronics and Communication Engineering, G. Pulla Reddy Engineering College (Autonomous), Kurnool, A.P, India*
[3]*Department of Electronics and Communication Engineering, JNTUA College of Engineering, JNTUA, Ananthapuramu, A.P, India*

Received 6 Jan. 2021, Revised 11 May 2021, Accepted 9 Jun. 2021, Published 9 Jan. 2022

Abstract: Diagnosis of cancer and its treatment is of widespread significance, because of the regular incidence of cancers and the frequency after treatment. The liver is the second organ most typically included by metastatic sickness, being liver disease the noticeable reason for death around the world. The early location of tumors is basic for the treatment of liver tumors. There are usually three different approaches to recognize liver cancer, such as blood tests, image tests, and biopsy. Computed tomography is a regularly used method for liver malignancy checking and treatment purposes. Automated liver tumor segmentation of CT images is a demanding problem. Image processing is applied to identify liver tumors. Image processing is a method of re-performing a few operations on an image. Steps for liver tumor segmentation using image processing includes image acquisition, preprocessing, liver segmentation, tumor segmentation, and classification. This article discusses the types, signs, symptoms, various tests for detecting tumors, stages of liver malignancy, and various image processing methods for tumor classification in the literature.

Keywords: CT Images, Liver Tumor, Liver Tumor Segmentation, Tumor Classification, Feature Extraction, Validation

1. Introduction

The main internal organ is the liver. It lies just under the right lung, and the right ribs. It contains two lobes as shown in Fig.1. Liver has various vital functions:

- It breaks down and provides the vitamins that the body must use to absorb from the intestines. Certain vitamins should be modified (metabolized) in the liver, not used as energy or used to structure and restore tissues.
- When there is cut or injured, it makes many blood clotting elements that prevent the body from bleeding out.
- It supplies bile into the intestines to assist take up vitamins (especially fats).
- In the blood, it breaks down alcohol, chemicals, and toxic waste that then passes from the body by stool and urine.

Numerous forms of benign (non-cancerous) and malignant (cancerous) tumors are developed by non-identical cells in the liver. Such tumors have various reasons, are treated diversely and have dissimilar diagnosis.

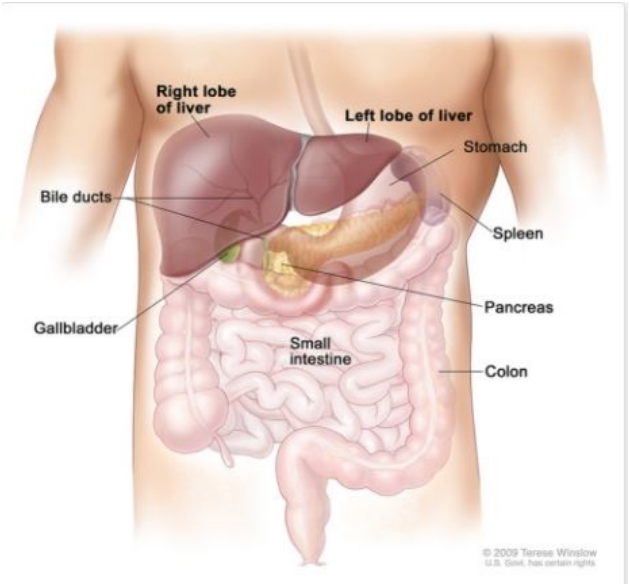

Figure 1. Structure of the Liver [1]

E-mail address: chagpraveena@gmail.com, suryakari2k9@gmail.com, prrjntu@gmail.com

A. Primary Liver Cancer (PLC)

PLC is called a cancer which originates in the liver. A couple of PLC exist.

1) Hepatocellular Carcinoma (HCC):

A well-known type of adult liver cancer (LC) is HCC. It have various patterns of growth:

- Some beginning as a solitary tumor which becomes bigger, extends to different portions of the liver in the advanced stages of the carcinoma.
- A second form tends to start as several small nodules of tumor in the liver instead of a single tumor. Persons with cirrhosis (chronic liver damage), that is seen most frequently and is a typical sample seen within the United States (US).

2) Intrahepatic Cholangiocarcinoma or Intrahepatic Bile Duct Cancer (IBDC):

IBDC is an about 20% of malignant growths that develop in the liver. These diseases begin in the cells inside the liver that line the narrow bile ducts. However, most IBDC truly originate external to the liver in the bile ducts.

3) Hemangiosarcoma and Angiosarcoma:

These are uncommon malignant growths that start in cells on the lining of blood vessels in the liver. Such cancers are guaranteed to spread in unprotected individuals from vinyl chloride or dioxide. It is suspected that there are added conditions due to the toxicity of radium or arsenic or caused by hereditary diseases are called hereditary hemochromatosis. These tumors develop rapidly, and they usually used for clinical resection when discovered. Radiation therapy can help to suppress the growth of disease, but difficult to diagnose these cancers

4) Hepatoblastoma:

It is an exceptionally uncommon cancer that arises in kids, normally in those under the age of 4. Hepatoblastoma cells are identical to the liver cells of the fetus. Approximately two out of every three children who have these tumors have been cured effectively with chemotherapy and surgery, but if they grow outside of the liver and are complicated to cure.

B. Secondary Liver Cancer (SLC)

It has not originated with the liver, but has developed from other body parts, which include the colon, pancreas, breast, stomach, or lung. It is called SLC, since this malignancy has extent from its initial (primary) source. For instance, cancer that originated in the stomach and expanded to the liver is known as stomach cancer, not LC. SLC are occurring frequently in the Europe and US than the PLC, whereas PLC is unexceptional in several areas of Africa and Asia.

1) Benign Liver Tumors (BLT):

Sometimes, BLT develop wide enough to begin complications, do not extent to distant areas of the body. Patients usually undergo surgery.

a) Hemangioma : This is the general form of BLT that originates in the blood vessels. The most of hemangiomas do not have any signs, so don't require treatment. But with surgery, some can bleed and necessarily discard.

b) Hepatic adenoma (HA): A BLT which begins with hepatocytes is HA. Most of them do not cause any symptoms and not require medication. But some ultimately show indications, such as abdominal soreness or a lump (stomach area) or loss of blood. As the HA will possibly burst (leading to significant loss of blood) and there is a slight danger that it will eventually grow into LC, doctors generally prescribe surgery to expel the tumor.

The incidence of HA is advanced by using some medications, such as women who use medications for birth control and men who take anabolic steroids have a danger of developing these tumors, but this is uncommon.

c) Focal nodular hyperplasia (FNH): Cancer cells development consisting of many types of cells such as bile duct cells, hepatocytes, and connective tissue cells is FNH. Both HA and FNH are usual in females compare to males.

2) Malignant Liver Tumors (MLT)

Metastatic is most dangerous tumor in the body. This spread from cancers in other body parts.

C. Key Statistics about LC

The projections for PLC and IBDC in the US by the American Cancer Society (ACS) for 2020 are:

- Around 42,810 new cases are identified (30,170 in males and 12,640 in females).
- Approximately 30,160 individuals are died from LCs (20,020 males and 10,140 females).
- Since 1980 to 2020, occurrence of LC has tripled, although the mortality rate has doubled.

Figure 2. Incidence rate of liver cancer globally [2]

Incidence rates for LC started to rise in the mid-1970s and are projected to increase by at least 2030. Globally, Key statistics of LC are shown in Fig.2. A research disclosed in JAMA Oncology in December 2017 found that between 1990 and 2015, the severity of LC is raised by 75% globally. In Asia and Africa, The LC occurrence is the highest, and the incidence in Mongolia far exceeds that of any other region.

New diagnoses of PLC and IBDC in the US are estimated by the ACS in 2020 to be approximately 12,640 in women and 30,170 in men (42,810 new cases). Globally, more than 800,000 individuals are identified with this disease every year. In maximum regions, each mortality and occurrence rates are 2-three times greater in guys; therefore, LC orders fifth in worldwide instances and 2nd in deaths of male. LC is now the rapidly growing reason of deaths due to LC in the US. Around 30,160 individuals (10,140 women and 20,020 men) will die from PLC and IBDC in 2020, the ACS reports. Internationally, with around 841,000 new cases and 782,000 annual deaths, LC was the sixth leading cancer diagnosis and the fourth growing risk of death from cancer in 2018 as shown in Fig.3.

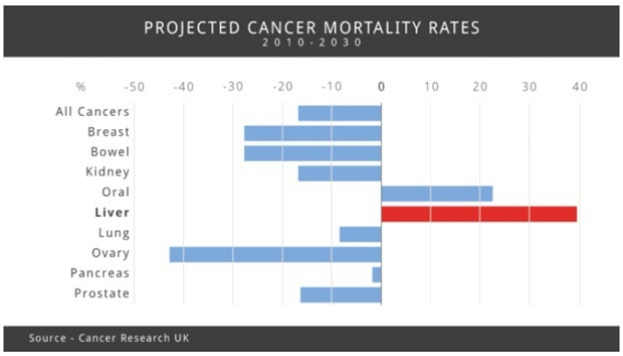

Figure 3. Mortality rate of different types of cancers in 2010-2030 [2]

D. Signs and Symptoms of LC

Symptoms typically do not arise until the progressive levels of the LC, but occasionally they can appear earlier. If the individual visit the doctor when signs are first detected, his or her LC is identified ahead of time, when care is more probably to be effective.

The signs of LC are:

- Loss of weight (without trying)
- Appetite loss
- Skin and eyes yellowing (jaundice)
- Feeling very complete after a tiny meal
- Vomiting or nausea
- Abdominal pain
- Swelling or build-up of fluids in the belly

E. LC Tests

Some LCs can be recognized by examining high-risk people who do not show symptoms (screening), but since they cause symptoms, most LCs are found. To look for indications of liver tumor (LT) and other medical problems, the specialist additionally investigates the patient, perhaps giving specific consideration to the midsection and testing the eyes and skin for jaundice.

1) Imaging Tests

These tests are utilized to produce images of the patient's internal organs by using magnetic fields, x-rays, or sound waves. Imaging tests can be conducted both before and after a LC diagnosis for a different reasons, such as:

- To assist in identifying suspect areas of cancer
- To assist a physician to direct a biopsy needle to collect a snippet of suspect area.
- To recognize how noticeably cancer could have spread
- Searching for any symptoms of cancer coming back following treatment

a) Computed tomography (CT): Several forms of LCs may be discovered with the abdomen CT scan. It may provide detailed knowledge regarding the size, location, and form of any tumor in the belly and surrounding blood vessels. If the CT scan is applied to target a biopsy needle accurately into an expected tumor region, then it is termed a CT-guided needle biopsy.

b) Ultrasound: The first procedure used to visualize at the liver is also an ultrasound. It produces an image on a computer screen using sound waves. This method exhibits tumors developing in the liver that can then, if necessary, be screened for cancer.

c) Magnetic resonance imaging (MRI): MRI give comprehensive pictures of the body's soft tissues. MRI scans utilize solid magnets and radio waves. MRI scans are useful in examining the LC. This can often tell a malignant tumor from a BLT. This is also utilized to observe blood vessels all around the liver and to see any blockages, which can assist whether the LT has expand to distinct organs of the body.

2) Biopsy

The withdrawal of a tissue sample to examine if it is cancer is a biopsy. Usually, a biopsy and examination in a pathology laboratory is the method used to ensure the existence of LC. But in some situations, biopsy is not required because imaging tests are used to determine whether the people are suffering from LC.

3) Alpha-Fetoprotein (AFP) blood test

AFP test is a protein, found in significant levels in grown-ups with liver infection, liver malignancy, who are pregnant, or different tumors. On the off chance that AFP levels are large in somebody with a LT, it likely to be an indication that liver malignant growth is available. However, liver disease isn't the main explanation behind high AFP levels. Numerous individuals with early liver malignant growth have typical degrees of AFP, so high AFP levels aren't useful in deciding whether a liver mass may be disease.

F. LC Stages

The cancer stage explains growth of LC in the body. It helps to decide the seriousness of LC and the best treatment. When considering survival rates, doctors often use cancer stages. These stages vary from stage 1 to stage 4. For the most situations, the lower the value, the smaller the malignant growth. A higher number indicates that the tumor has advanced further, such as stage 4. Different physicians use different staging schemes for LC. The popular cancer staging system is TNM.

The union for international cancer control establish the TNM classification system as a way for physicians to establish several different forms of tumor based on certain guidelines.

In the TNM system, the complete stage is calculated after a letter or number is assigned to the cancer to identify the categories of tumor (T), node (N), and metastasis (M).

- The size of the cancer (T): tells about how big the tumor has size and it is shown in Fig. 4, or is there couple of tumor or has the cancer entered to the tissues close by.
- Transmission to neighboring lymph nodes (N)
- Metastasizing to distant sites (M)

Figure 4. Comparison of Sizes of Liver Tumor [1]

More information on each of these variables is given in the letters or numbers after T, N, and M. Higher numbers indicate a more advanced tumor. If the categories T, N, and M of an individual have been identified, this details are integrated to assign an overall stage is called stage grouping, as shown in the Table I [3].

2. Related Work

Megha Ganjre et al. [4], developed a technique wherein they used morphological capabilities (erosion) in pre-processing to reduce computation time and efforts with the aid of getting rid of more regions and segmentation of liver is completed using region growing approach. The principle disadvantage of region growing method is manual seed point identification. If this seed point is not positioned well, it is able to result in false segmentation.

Dirk Smeets et al. [5], segmented LTs by two manually located points. The main segmentation is done by considering the tumor center and extreme radius computed from these two points using spiral scanning technology. The level set method uses the speed function obtained by using the pixel classification algorithm to adjust this first segmentation. This algorithm is more effective for tumors with obvious edges, large difference in average gray intensity between tumor and liver, and small standard deviation of the two intensity distributions. In addition, users are required to have some knowledge about tumors.

Munipraveena rela et al. [6], proposed an opposition-based spotted hyena optimization (O-SHO) for LT segmentation and classification. Images are pre-processed with histogram equalization (HE) and noise filtering, then level set segmentation is applied for liver segmentation (LS), then fuzzy centroid-based region growing algorithm is applied for LT segmentation. Finally, Image is classified as tumor infected and non-infected region by using CNN and RNN with O-SHO optimization. The experiment results designate that the accuracy achieved is efficient, and less effected by noise.

Ye Yuana et al. [7], integrated the advantage of superpixel, random walk and active contour algorithms for organ segmentation. New superpixel algorithm, a compact watershed for contrast enhancement is employed as a pre-processing to minimize the processing time. To enhance accuracy, an improved narrow-band active contour model was established. Knowledge-based random walk segmentation is used, which avoids the laborious 2D segmentation annotation work and the time utilization of 3D segmentation. This model is accurate and effective.

Yang Li et al. [8], established a technique which depend on level sets, sparse shape components (SSCs) and graph cuts for LS. It can effectively deal with normal liver and pathological liver without complicated training process. These capabilities are proved by the following evidence. Firstly, a level set method merging intensity deviation field and location constraint is utilized. The intensity deviation adjust the intensity unevenness in the evolution of the level set, and location constraint can limit the possibility of misclassification of unrelated organs. In order to validate ultimately extracted pathological liver shape, an SSC-based algorithm is proposed, and then the graph cut is implemented. Liver optimization is carried out through intensity terms, boundary terms and location constraints. Experiments showed that LS method has proven to be superior to some existing methods.

TABLE I. TNM Staging System

Stage	Grouping	Explanation
IA	T1a-N0-M0	T1a: A lesion of 4/5 inch (2 cm) or smaller.
IB	T1b-N0-M0	T1b: One lesion of size larger than 4/5 inch (2cm).
II	T2-N0-M0	T2: A lesion greater than 2 cm has developed into a blood vessel,or a couple of lesion but no longer large than 5 cm (approximately 2 inches)
IIIA	T3-N0-M0	T3: A couple of lesions, or minimum one lesion larger than five cm
IIIB	T4-N0-M0	T4: Minimum one lesion which has developed into hepatic vein.
IVA	Any T-N1-M0	One lesion or couple of lesions of any size which has expand to nearby lymph nodes but not to other organs.
IVB	Any T-Any N-M1	One lump or couple of lumps of any size and would or won't have developed to close by lymph nodes. It has extended to various organs, for example, the lungs or bones.

N0 and M0: Tumor did not extend to lymph nodes and distant organs.

Abdul Qayyum et al. [9], developed a 3D residual network (RN) with a spatial squeeze and channel excitation (cSE) block for LS. This system utilizes cSE blocks to obtain spatial information by using the reweighting function in a three-D RN. The network was analyzed on different dataset and showed that the cSE-RN provides good overall performance in medical segmentation.

A.M. Anter et al. [10], proposed a technique for segmentation using neutrosophic set (NS), particle swarm optimization (PSO) and fast fuzzy C-means algorithm (FFCM). Initially, the median filter (MF) is applied to regulate the intensity values and eliminate excessive frequency of the CT image. Subsequently, the CT image is changed to the NS domain. Then, Entropy is calculated to measure the uncertainty within the NS domain. Then, PSO is implemented to progress the NS image to the optimized FFCM to enhance, optimize the clustering outcomes and segment the liver from CT using PSOFCM technology.

Anter, A.M. et al. [11], integrated watershed algorithm, NS and FFCM for segmentation. Initially HE and MF methods are applied to adjust the intensity value and remove high frequencies. The CT image is then modified to the NS domain. The NS image is improved by adaptive threshold and morphological operators. The connected component method is implemented to separate the liver region, then the watershed algorithm is applied to perform the post-segmentation process. Lastly, the FFCM is employed to segment the LT.

A.Baazaoui et al. [12], presented a method which utilizes an entropy-based fuzzy region growth to segment LTs with reducing leakage, especially in CT images that include multiple lesions. Starting from manually selected seed pixels, this method iteratively calculates the average entropy of the region, and uses a fixed threshold-based membership to obtain the final tumor region. The intersection between adjoining tumors is processed by distance-based processing in the presence of several tumors within the one CT image, so that each pixel is especially allocated to at least one tumor.

Lei Xu et al. [13], suggested an approach which includes three stages to remedy the problems of leakage and excessive segmentation. First, the original input image is pre-processing via a chain of techniques to reap a binary image. Then set some seed factors used for region growth to acquire a binary image of the liver contour. Subsequently, a new stage set active contour model is established for LS. Initially, the gradient amplitude of the input image is filtered by using gaussian characteristic for edge enhancement and noise reduction. In addition, depend on the gradient information of the image, a binarization technique is proposed to choose the best threshold without manually placing parameters. Finally, both local and global information can be integrated by a new signed pressure function.

Xing Zhang et al. [14], developed a LT segmentation that integrates watershed transformation and SVM classification. This approach was examined with the abdominal CT volume of 10 liver tumors, and 5 quantitative indicators are measured. The average overlap error of 10 tumors was 31.14% . This method is accurate and effective for many types of tumors.

Munipraveena rela et al. [15], utilized a superpixel-based FFCM clustering for LT segmentation. To obtain segmentation accuracy, multiscale morphological gradient reconstruction based superpixel is used. FCM with improved object is implemented to acquire the LS and is fast and accurate.

3. LT Classification based on Image Processing (IP)

IP is utilized as a non-intrusive technique to distinguish LTs. The advancement of IP methods has stimulated a plenty of research work aimed at developing computerized methods for automatic liver analysis. The steps used for the tumor classification is shown in Fig. 5

A. *CT Images*

CT examines are utilized to characterize ordinary and unusual structures of the body parts or potentially help

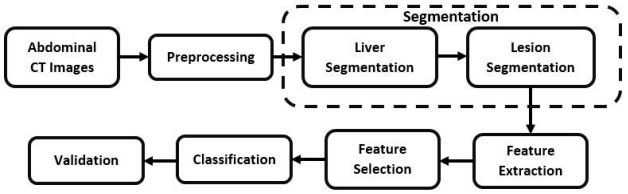

Figure 5. Steps for liver tumor Classification

techniques by serving to precisely direct the position of instruments or medicines. This is an imaging method which uses tomography. Tomography is a technique of generating a tomographic or sliced two-dimensional image (tomogram) from a three-dimensional object. An abdomen CT scan is advantageous in deciding the anatomy of human organs, including visualization of the liver, gallbladder, spleen, pancreas, aorta, and kidneys. To check the existence of tumors, infections, abnormal anatomical structures or physical changes caused by trauma, a CT scan of this area was used [16].

1) Datasets

Presently accessible public datasets incorporate MIDAS dataset 2016, IRCAD dataset 2016, CIR dataset 2016, and Sliver07 dataset 2016 [17].

B. Preprocessing

Preprocessing is the preliminary step required to obtain accuracy of segmentation. CT images contain noise, which diminishes the overall accuracy of the image. First convert the image to grayscale image, and then apply a MF to eliminate noise. 3D anisotropic diffusion is also applied to remove image noise. The filter also retains important structures, in particular lines, edges, and other details that are significant for interpreting the image. The disadvantage is that this filtering method demands more calculation time because of the iterative process. The curvature anisotropic diffusion image filter can smooth CT images to reduce some noise [18].

IP serves a vital position in suppressing the noise of CT images. Noise reduction is a process of removing the noise exist in the image and minimizing the loss of features in the noise eliminated image. Using previous perception of CT images and noise, CT image noise reduction can be performed better [19]. IP techniques used in literature are shown in Fig. 6 and Table II. Images can usually be denoised using: (i) spatial and (ii) transform domains.

1) Spatial Domain Filtering [20]

It is a conventional technique to eliminate noise from an image. By directly applying filtering to the original image, spatial filters minimize noise. These filters are typically distinguished into linear and non-linear filters.

a) Linear and Non-linear filters: Linear filters are applied to reduce the noise, but they are not effective in maintaining image details. Mean filtering is applied to

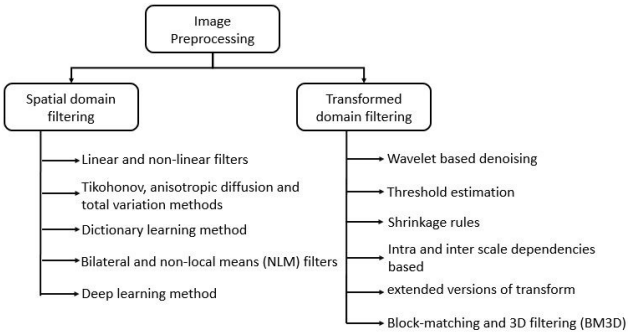

Figure 6. Techniques for image preprocessing

reduce gaussian noise, and this filter produce blurred image for high noise. To solve this problem, wiener filtering is applied. Non-linear filters for example MF can eliminate noise without any attempt to clearly identify them.

Median filter (MF) substitutes the center pixel of the rectangular window with the median pixel value of the rectangular window, as shown in (1)

$$\hat{g}(i,j) = \underset{(p,q)\in S_{ij}}{median}\{f(p,q)\} \tag{1}$$

S_{ij}, subimage, represent a $m \times n$ rectangular window, (p,q) is the center of the window. $f(i,j)$ is input image in the S_{ij}. $\hat{g}(i,j)$) is median filtered image.

Wiener filter (WF) [21] is employed for images degraded by blurring and additive noise. $X(f1,f2)$ is frequency domain description of corrupted image $x(n,m)$. The filtered image $\hat{S}(f1,f2)$ can be obtained by multiplying $X(f1,f2)$ with the WF $G(f1,f2)$ as in (2), where WF is represented in (3):

$$\hat{S}(f1,f2) = G(f1,f2)X(f1,f2) \tag{2}$$

where

$$G(f1,f2) = \frac{P_s(f1,f2)}{P_s(f1,f2)+\sigma_n^2} \tag{3}$$

$P_s(f1,f2)$ fourier transform of the signal autocorrelation, σ_n^2 is variance of noise

Gaussian filter (GF) is applied to 'blur' images and eliminate details and noise. It is like the mean filter in this specific situation, but it makes use of a special kernel that reflects the form of the gaussian. The 2D isotropic gaussian is given in (4).

$$G(p,q) = \frac{1}{2\pi\sigma^2} e^{-\frac{p^2+q^2}{2\sigma^2}} \tag{4}$$

b) Bilateral filter (BF): BF is a non-linear filter, restore edges and eliminate noise. Each pixel of an image has been substituted by a weighted mean of neighboring pixel values. The BF is represented as in (5).

TABLE II. VARIOUS MEDICAL IMAGE ENHANCEMENT METHODS

Ref	Methodology	Parameters measured	Remarks
[23]	Spatial domain method, use the parameter $K = \frac{\sum_{i=1}^{m}\sum_{j=1}^{n} x(i,j)}{m \times n}$ $EI = \frac{[x - min(x)] \times e^{K}}{[max(x) - min(x)]}$	Universal Image Quality Index (UIQI)	Fast implementation and depends on the normalization technique not on histograms
[24]	Using DWT and SVD	Mean, STD, PSNR, WPSNR, QRCM	Edge information is preserved by unchanging high frequency details of image, but low frequency image details are transformed.
[25]	Fusion rules applied on Gaussian filtered image and gradient image	Entropy, PSNR, SSIM	Enhancement of low contrast images.
[26]	A NLM filter and correlation-based wavelet packet thresholding	PSNR, IQI, ED	Appropriate for two similar images with uncorrelated noise.
[27]	Modified Haar wavelet transform and image fusion.	MSE, PSNR, MI, UIQ	Combine images obtained using PET and CT scan.
[28]	Low-rank sparse component decomposition and dictionary learning.	MI, Tsallis entropy, nonlinear correlation	Simultaneous fusion, denoising, and enhancement of multi-modal medical images
[29]	The merits of fractional differential and directional derivative.	Mean, clarity entropy	The texture information of the image is enhanced. The best fractional differential order is $\alpha = 0.8$, it improves both the high and the low frequency image information.
[30]	A dynamic unsharp masking using optimum wavelet based masking.	Absolute Mean Brightness Error (AMBE)	Unsharp masking technique
[31]	A new penalized weighted least squares reconstruction method that exploits regularization based on an Efficient Union of Learned TRAnsforms.	RMSE, SSIM	For low-dose CT imaging

$$BF\,[X]_i = \frac{1}{N_i} \sum_{j \in S} G_{\sigma_s}(\|i-j\|)\, G_{\sigma_r}\left(X_i - X_j\right) \tag{5}$$

N_i is called normalization factor as shown in (6):

$$N_i = \sum_{j \in S} G_{\sigma_s}(\|i-j\|)\, G_{\sigma_r}\left(X_i - X_j\right) \tag{6}$$

G_{σ_i} is the 2D gaussian function as in (7)

$$G_{\sigma}(i) = \frac{1}{2\pi\sigma^2} exp(-\frac{i^2}{2\sigma^2}) \tag{7}$$

The filtering magnitude is specified by σ_s and σ_r for image X. G_{σ_s} is a gaussian spatial factor that decreases the influence of distinct pixels, G_{σ_r} is a gaussian range that lowers the impact of j pixels when their intensity values vary from X_i.

c) Non-local mean (NLM) filter: NLM is weighted by how close they are to the target pixel, takes the mean of all pixels in the image. Compared to mean filtering, applying this filter will give improved post-filtering clarity with reduced loss of information. In specific circumstances, first option for smoothing noisy images should be the NLM or BF.

d) Anisotropic diffusion filter (ADF): With regards to image processing, the ADF has been effectively used to eliminate high frequency noise while retaining the main edges of existing artifacts. ADF is an iterative algorithm in its discrete form that simulates the diffusion process by (8):

$$I_{x,y}^{t+dt} = I_{x,y}^{t} + \frac{dt}{|N_r|} D \sum_{(p,q) \in N_r} (I_{p,q}^{t} - I_{x,y}^{t}) + dt \times f(X_{x,y}^{t}) \tag{8}$$

Where D denotes a diffusion coefficient and a nonlinearity $f(I)$ is represented by (9)

$$f(I) = -\beta I(I-a)(I-1) \tag{9}$$

β controls the degree of nonlinearity, a is referred to as the nonlinearity threshold, $N \times M$ corresponds to the size of image, and $|N_r|$ represents the 4 neighbors, other than the boundaries of the image. In addition, N_r =

$(p-1,q),(p+1,q),(p,q+1),(p,q-1)$ is the set of neighbors. In addition, at time step t, $I^{t}_{x,y}$ indicates the filtered image grey level, while at the next time step, the grey level is $I^{t+dt}_{x,y}$.

2) Transform Domain Filtering [22]:

Wavelet is a function used to decompose an image into various components of frequency. Wavelet transform has emerge as a technology for image processing applications because of its limitations in frequency, sub-band, multi-resolution analysis and time domain.

a) Wavelet transformed based denoising: Two parameters should be specified in the DWT. Firstly, for decomposition, a wavelet function is used. The decomposition can be performed by the following filters of wavelet decomposition: harr, meyr, etc. Next for thresholding all sub bands, the decomposition rate is chosen.

In the wavelet domain, the WF produces better results when there is gaussian noise in the picture. This filter, however, did not yield visually agreed results, but the MSE was effectively reduced by the filtering operation.

In wavelet transformed denoising, the non-linear approach using thresholding is the other best method. Large wavelet coefficients are not disrupted and by using threshold value, eliminate wavelet coefficients which are small in high frequency sub-bands. Thresholding strategies are employed to eliminate undesirable values, preserve large coefficient values, and eliminate noise.

To determine the distribution of intensity values in the image, histogram techniques are applied to obtain the valleys, peaks, and curvatures. As a probability distribution function, the histogram of the background and foreground can be interpreted as two gaussian distributions. Thresholding can be achieved by entropy based approach.

b) Non-subsampled contourlet transform(NSCT) based enhancement: The NSCT is the enhanced contourlet transform that can solve the issue of artefact creation within the enhanced curve picture in an excellent way. In addition, choosing the output of the enhancement as well as the NSCT filter will directly affect the impact of image enhancement. The NSCT decomposition is shown in Fig. 7.

c) Threshold estimation: For edge enhancement and noise elimination, the choice of a threshold value for CT image is very difficult. If this value is small, then the noise is not completely removed. If this value is high, then the image will become blurred. To determine the acceptable threshold value, there are different algorithms used. SureShrink, BayesShrink, and VisuShrink are three strategies for threshold estimation.

The SureShrink threshold is based on the adaptive threshold of a sub band. For each sub-band, Steins uses

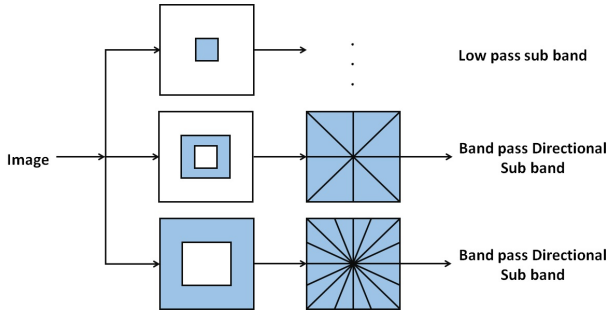

Figure 7. The diagram of the NSCT decomposition

an impartial risk estimator to achieve a different threshold (SURE). In order to obtain the threshold, BayesShrink uses a bayesian computational method and performs a simplified gaussian distribution for the wavelet coefficients in every comprehensive sub band.

VISUShrink is a non-adaptive global threshold that has one threshold value, and this value is derived from all the image pixel values. For all decomposition levels, this global threshold is used. By using the VisuShrink process, the input image is over-smoothed.

d) Block-matching and 3D filtering (BM3D): BM3D is applied for images degraded by additive white gaussian noise. BM3D is a powerful filtering in three-D transform area via manner of integrating sliding-window rework processing with block-matching. Blocks inside the image are analyzed in a sliding way and implemented the block-matching idea through figuring out for blocks that are just like the one presently analyzed. The matched blocks are stacked collectively to shape a 3D array and the records inside the array suggests a robust degree of correlation because of the similarities among them. By employing a 3-d decorrelating unitary transform, this association is exploited and the noise is successfully diminished via shrinking the transform coefficients. The ensuing inverse three-D transforms the approximate yields of all the blocks matched. The ultimate approximation is decided as a weighted imply of all overlapping block estimates after iterating this technique for all image blocks in a sliding manner.

C. Segmentation

LC causes serious deaths worldwide. In helping surgeons and doctors, computer-aided diagnosis and liver surgery planning systems are now playing a crucial role. Accurate and automatic segmentation methods of liver, blood vessels, and tumors are essential for computer-aided liver disease diagnosis, liver surgery planning systems, and liver transplantation systems. But, because of the excessive changes inside the form of the liver, the low contrast and intensity of uniformity inside the liver, the weak borders with adjacent organs such as the stomach and heart, and the uniformity of intensity with adjacent organs as shown in Fig. 8, liver segmentation (LS) has become a difficult task, attracting more research. LS from abdominal images is a

method of subdividing CT images into liver parenchymal regions and non-parenchymal regions.

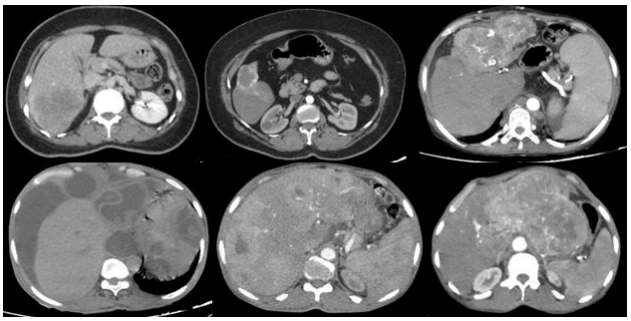

Figure 8. Abdominal CT images

LS methods are classified into three key groups, including the grey level based, structure based and texture based methods as shown in Fig. 9 [32]. Various image segmentation methods used in literature are listed in Table III.

1) Gray Level Based Methods:

a) Region-based segmentation (RBS): As RBS consists of the selection of preliminary seed points, it's also categorized as a pixel-based segmentation technique. This segmentation method analyses the neighboring pixels of the initial seed point and decides whether or not the region must be brought to the pixel neighbors. The technique is iterated on in the equal way as algorithms for popular data clustering.

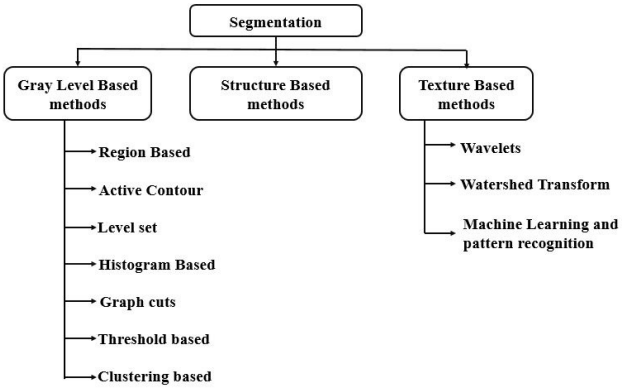

Figure 9. Techniques for tumor segmentation

Choosing a bunch of seed points is the initial phase in growing the region. A seed point is selected for pixels in a certain grayscale range. Depending on pixel intensity, the area is then developed from the seed pixel to adjoining pixels. The area is shaped by the use of 4-connected or eight-connected neighborhoods from the seed point. If adjoining seed point pixels have the equal seed point intensity value, then those pixels are labeled as seed points. In two successive iterative levels, this manner continues till there may be no alternate. The primary goal of region growth is to categorize the image's similarity into regions

b) Active contour models (ACM) [33]: ACM is a segmentation method which may be certain for similarly processing and evaluation as the utilization of energy forces and constraints for the segregation of the pixels of concern from the image [34]. The standard utilization of active contours is to provide an explanation for the smooth shape of the image and the outlines of the area's closed contours. ACMs involve snake version, gradient vector go with the flow snake version, balloon model and geometric or geodesic contours. A parametric curve that may travel inside a spatial image domain in which it has been specified is the standard ACM, also called snake. The curve is described by $x(s,t) = (p(s,t), q(s,t)), s \in [0,1]$, here E develops to decrease the whole energy described by means of the subsequent as in (10):

$$E_{snake} = \int_0^1 [E_{int}(x(s,t)) + E_{ext}(x(s,t))]\, ds \qquad (10)$$

This energy function involves two distinct energies: E_{ext} is the external energy denoted by the image's specific gradient characteristics, and E_{int} is internal energy that controls the curve's shape modification and to continue the search inside the image. Alternatively, the standard ACM's execution contains a set of N discrete points $\{x_n \mid n = 1, 2, 3, ..., N\}$, and the local energy function is denoted by (11), that is repeatedly assessed to limit the s_n index in the W_n search window for the actual discrete point using the iteratively evaluation (12)

$$E_{(n,m)} = E_{int} + E_{ext}$$

$$E_{snake} = \sum_{n=1}^{N} E_{n,s_n} \qquad (11)$$

$$s_n = \underset{m}{argmin}(E_{n,m}), m \in W_n \qquad (12)$$

The standard ACM has the disadvantages of initialization and local minimum issue [35].

c) Threshold [36]: It is frequently applied method in segregating against the background in the foreground. The gray image is changed to a binary image by considering an appropriate threshold value, T. All important details about the location and shape of objects of interest should be comprised in the binary image (foreground). The binary image reduces the data complication and simplifies the identification and classification process. Selecting a single threshold value (T) is often familiar way to transform a gray-level image to a binary image. Then all the gray levels lower than T will be listed as black (0), and white (1) will be those higher T. The challenge of segmentation is the one choosing the accurate threshold T. A usual method to pick T is by examining the histograms of the image which

TABLE III. VARIOUS MEDICAL IMAGE SEGMENTATION METHODS

Ref	Methodology	Parameters measured	Remarks
[40]	A deep learning model, namely SegNet	Accuracy, TPR, Specificity, IoU	Need to improve localization accuracy of the tumor
[11]	HE, MF, NS domain, morphological operators, watershed algorithm, the connected component, FFCM algorithm	Entropy-based metric, dice coefficient, Jaccard Index,	NS has more information than Fuzzy Logic.
[10]	NS, FFCM and PSO.	The Jaccard Index, The Dice Coefficient, ANOVA	Requires more computational time
[41]	The segmentation results of FCM and extreme learning machine are fused by adaptively calculated weights.	VOE, RVD, ASD, RMSD	LS is not accurate due to irregular intensity difference between liver and lesion.
[42]	Confidence connected region growing algorithm, improved FCM and graph cuts	VOE, RVD, ASD, RMSD, MaxD, DICE.	This method gives under segmentation and over segmentation errors
[15]	Superpixel algorithm for preprocessing, and FCM for segmentation	GLCM	Semi-automatic method
[58]	FCN and non-negative matrix factorization based deformable model.	VOE, RVD, ASD, RMSD, MSD.	Failed for the tumors with low contrast and little intensity difference
[59]	Multi-scale candidate generation method, 3D fractal residual network, and ACM	VOE, RVD, ASD, MSD.	Multiple tumors adjacent to each other are segmented to one tumor and Tumor boundaries cannot be segmented precisely.

need to be segmented. Histograms are more complicated in actual applications, with several peaks and valleys not simple, and T value is not always easy to pick.

d) K-means clustering [37]: The method detects classes in the data, with the number of classes being described by the variable K. Depending on feature similarity, the algorithm allocates every pixel to one of the classes. Clustering works iteratively to shape groups organically, rather than examining predefined groups.

e) Histogram-based image segmentation: This technique utilizes a histogram focused on "gray levels" to group pixels. Simple images compose of a background and an object. Two different gray levels are used to represent background and object. Since background is larger compare to object, it is represented by major peak in the histogram of image.

f) FCM clustering: The study of clustering refers to the subdivision of image I into c sub-sets called clusters, which are diverse and non-empty. The mixture of these clusters generates the image I. The membership function is utilized to illustrate the likeness between pixel and cluster, and has the value between [0, 1]. If the membership is one then the pixel and the cluster are extremely similar. If membership is near zero, then the correlation between the pixel and the cluster is very low. Let $I = \{ i_1, i_2, \ldots\ldots, i_N\}$ be N observations in an Euclidean space; i_k is the k-th feature vector; i_{kj} the j-th feature of i_k. If c is an integer, $2 \leq c \leq N$, A conventional c-partition of I is a c-tuple $(I_1, I_2, ..., I_c)$, subsets of I that fulfil (13), (14), and (15) as given below:

$$I_n \neq \emptyset; 1 \leq n \leq c; \tag{13}$$

$$I_n \cap I_m = \emptyset; n \neq m; \tag{14}$$

$$\bigcup_{n=1}^{c} I_n = I \tag{15}$$

Let $P = [p_{ik}]$ be a $c \times N$ matrix, P is the matrix description of I_n in (13), it is represented as in (16), (17), and (18).

$$p_n(i_k) = p_{nk} = \begin{cases} 1; & i_k \in I_n \\ 0; & otherwise \end{cases} \tag{16}$$

$$\sum_{n=1}^{N} p_{nk} > 0; \text{for all n;} \tag{17}$$

$$\sum_{n=1}^{N} p_{nk} = 1; \text{for all k;} \tag{18}$$

The generalized least-squared errors approach as shown in (19) is suggested for understanding fuzzy c-partitions in I.

$$J_s(P,q) = \sum_{k=1}^{N}\sum_{n=1}^{c}(p_{nk})^s \|i_k - q_n\|_A^2 \quad (19)$$

Where s weighting exponent; $1 \le s < \infty$, P is fuzzy c-partition of I; $q = (q_1, q_2, ..., q_c)$ = vectors of centers; $q_n = (q_{n1}, q_{n2}, ..., q_{nN})$ = centers of cluster i, A is $N \times N$ positive-definite weight matrix, $\|\cdot\cdot\|_A$ is induced A-norm, d_{nk}^2 is the squared distance between i_k and q_n as shown in (20)

$$d_{nk}^2 = \|i_k - q_n\|_A^2 = (i_k - q_n)^T A(i_k - q_n) \quad (20)$$

For $s > 1$, if $i_k \neq q_m$ for all k and m, $(\hat{P}, \hat{q})$ may be locally optimal for J_s only if $\hat{q}_n$ and $\hat{p}_{nk}$ are as described in (21) and (22).

$$\hat{q}_n = \frac{\sum_{k=1}^{N}(\hat{p}_{nk})^s i_k}{\sum_{k=1}^{N}(\hat{p}_{nk})^s}; 1 \le n \le c; \quad (21)$$

$$\hat{p}_{nk} = \left(\sum_{m=1}^{c}\left(\frac{\hat{d}_{nk}}{\hat{d}_{mk}}\right)^{\left(\frac{2}{s-1}\right)}\right)^{-1}; 1 \le k \le N; \quad (22)$$

f) Graph-cut method (GCM) [38]: The GCM describes the problem of segmentation into a minimization of a Gibbs energy as given in (23)

$$E(L) = \lambda \sum_{p \in I} R(x, L_x) + \sum_{\{x,y\} \in N} B(x,y)\delta\left(L_x \neq L_y\right) \quad (23)$$

Where $\delta\left(L_x \neq L_y\right) = \begin{cases} 1; L_x \neq L_y \\ 0; L_x = L_y \end{cases}$, N is neighboring pixel pairs $\{x, y\}$ in the image, I is a set of pixels in an image, and L_x is a binary value allotted to pixel x indicating the object ($L_x = 1$) or the background ($L_x = 0$). $\lambda, \lambda \ge 0$, is regularizing factor describes the significance of the region parameter $R(x, L_x)$ beside the boundary parameter $B(x, y)$. $R(x, L_x)$ is defined in (24):

$$R(x, L_x) = -lnPr(I_x \mid L_x) \quad (24)$$

Where $Pr(I_x \mid L_x)$ is the probability of the intensity I_x by L_x, and I_x is the intensity of x. Thus, $R(x, L_x)$ reflects the probablity that x belongs to L_x. Then, $B(x, y)$ is defined in (25).

$$B(x,y) = \frac{exp\left(-\frac{(I_x - I_y)^2}{2\sigma^2}\right)}{\|x - y\|} \quad (25)$$

Where σ is the noise standard deviation, and $\|x - y\|$ is the euclidean distance between x and y. A graph demonstrating the energy characteristic in (23) includes the pixel node, the object node, and the background node. Three steps are utilized for the edges joining these nodes. Initially, edge weighting factors of $R(x, 0)$ and $R(x, 1)$ are used to attach every pixel node as the object and background nodes, respectively. Each neighboring pixel node pair for x and y is attached with an edge weighting component of $B(x, y)$. In the end, the pixel nodes, which might be allocated to the object and the background seed by way of the human interaction, are linked to the object and the background node.

2) Structure Based Methods:

In several medical applications, structure-based approaches have proven to be efficient and strong. The fundamental hypothesis is that there is a repeated type of geometry in the structures of interested objects. A probabilistic model is developed in the approach to reflect the variety of organ shapes and to use this concept as basic information to inflict constraints on a segmentation image.

3) Texture Based Methods:

Methods based on texture don't concentrate on object boundaries, and consider the texture features instead. The primary process is: first, the target's texture characteristics are determined; then a classifier is used to classify the characteristics; lastly, post-processing refines and smooth the target region.

a) Watershed algorithm [39]: In geography, the ridge that separates areas drained by more than one river structures is a watershed. The transform of the watershed is a segmentation technique depending on morphological gradient. The image's gradient map is understood to be a relief map wherein exclusive values of the gradient correspond to distinct heights. The water level could rise over the basins if we punch a hole at every nearby minimum and immerse the complete map in water. A dam is shaped among them when separate bodies of water meet.

The development continues until all of the points are immersed in the map. Ultimately, the entire image is segmented through the dams which can be then considered watersheds, and the catchment basins are called the segmented areas. The geographic place which drains right into a river or reservoir is a catchment basin.

b) Machine learning and pattern recognition: In order to know what's within the image, several computer vision tasks involve intelligent segmentation of a picture to permit for easier analysis of every element. The image segmentation methods of today use deep learning (DL) models

to fully understand which pixels are used to express the real-world. Modern techniques for image segmentation are driven by DL technology, which includes:

Convolutional Neural Networks (CNNs): CNN image segmentation requires providing parts of an image to a CNN that marks the pixels as an input. The complete image cannot be processed at once by CNN. It examines the image, each time observing at a tiny filter of a number of pixels, until the perfect image has been mapped.

Fully Convolutional Networks (FCNs): There are completely connected layers in conventional CNNs, which do not accommodate dissimilar input sizes. FCNs utilize convolutional layers to operate on dissimilar input sizes and activate quickly. There is an extensive receptive area inside the last output layer which coincides to the width and height of the image, even as the wide variety of channels indicate the variety of categories. With the intention to decide the context of the image, together with the location of artifacts, every pixel is categorized by the convolutional layers.

Ensemble learning (EL) synthesizes the outcomes into a single distribution of two or more similar analytical models. EL can enhance the accuracy of prediction and reduce errors in generalization. This allows for precise classification and segmentation of image. Rather than seeking to create a specific ideal learner, EL segmentation create a set of poor base-learners that identify parts of the image and integrate their performance.

DeepLab: One key inspiration for DeepLab is to achieve image segmentation whereas serving to monitor signal decimation which the network should process. Other motive is to permit learning of multi-scale contextual features, combining features at different scales from images. DeepLab needs pre-trained complete residual neural network (ResNet) for feature extraction. Rather than regular convolutions, DeepLab utilizes atrous convolutions. The various dilation rates of every convolution permit the ResNet to record contextual data on more than one scales.

SegNet Neural Network: A primarily-based deep encoder and decoder structure, also called semantic pixel-wise segmentation. It needs encoding the input's low dimensions and then restoring it with orientation invariance capabilities within the decoder as shown in Fig. 10. This produces a segmented image at the decoder's end.

D. Feature Extraction (FE)

FE enables to moderate the variety of characteristics in an image by producing novel features from existing ones (after which neglecting the existing features). This updated, simplified series of features need to then be able to sum up the various details enclosed in the existing features. Like that, a recapitulated model of the existing features may be produced from a mixture of the original collection.

Extraction of features is the name of the method of selecting and/or merging variables into features, which essentially decreases the required data to be processed, while also expressing the original data set accurately [43]. Types of features extracted are shown in Fig. 11.

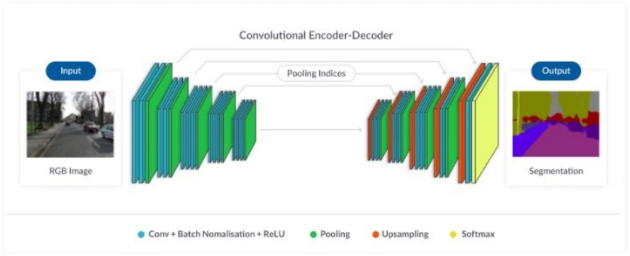

Figure 10. SegNet Neural Network [37]

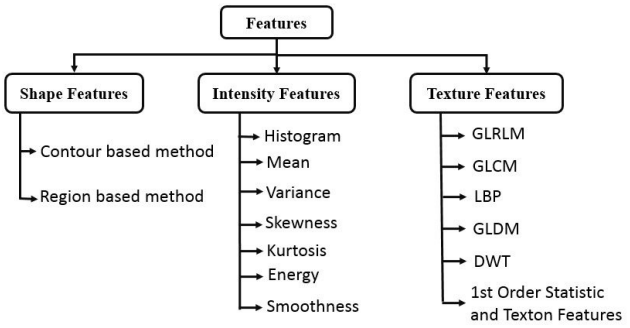

Figure 11. Types of Features

1) Shape Features:

These are classified as region based and contour based features.

a) Region based features: Essentially, Region-based features include the measuring of relationship between shapes described by means of their features. Some easy geometric capabilities are utilized to explain shapes [44].

Center of gravity or centroid (26): Its location need to be stable with regards to the shape. Matlab code is I=bwlabel(bwimage,8); stats=regionprops(I,'Centroid'); Cent=[stats.Centroid]; where bwimage is binary image.

$$\begin{cases} g_x = \frac{1}{N}\sum_{i=1}^{N} x_i \\ g_y = \frac{1}{N}\sum_{i=1}^{N} y_i \end{cases} \tag{26}$$

(g_x, g_y) is the centroid of an image with (x, y) denotes pixel location

Circularity ratio (27): This symbolizes however a shape is analogous to a circle. It is given by (27)

$$C_2 = \frac{A_s}{o^2} \tag{27}$$

Where A_s is the area of a shape, and o is perimeter of

a shape.

Matlab code: Stats=regionprops (L,'Area', 'perimeter'); ar = [stats.Area]; per = [stats.Perimeter]; Cr=ar/(per*per);

Rectangularity (28): It describes that what proportion of image covers its smallest bounding rectangle.

$$Rectangularity = \frac{A_S}{A_R} \tag{28}$$

Wherever A_R is that the area of the smallest bounding rectangle. MatLab Code: Stats=regionprops(L,'Extent'); rectangularity=[stats.Extent];

Convexity(29): It is outlined as the quantitative relation of the convex hull to the initial contour.

$$convexity = \frac{o_{convexhull}}{o} \tag{29}$$

Stats=regionprops(L,'perimeter','Conveximage"); pShape = [stats.Perimeter]; Cimag = stats.ConvexImage; Cimg = double(Cimag); s=regionprops(Cimg,'perimeter'); pHull = s.Perimeter; cvx = pHull/pShape;

Solidity: It represents the degree to that the shape is convex or concave as in (30).

$$solidity = \frac{A_s}{H} \tag{30}$$

Where, H is that the convex hull space of the shape. Stats=regionprops (L,'Solidity'); solid = [stats. Solidity];

Euler number (31): It denotes the relation between the number of contiguous elements S and also the number of holes N on a shape.

$$\text{Euler number} = S - N \tag{31}$$

Stats=regionprops (L,'Euler'); EN = [stats.Euler];

Hole area ratio (HAR) (32): HAR is described as

$$HAR = \frac{A_h}{A_s} \tag{32}$$

Where A_h is the total area of all holes in the shape.

b) Contour based features [45]: Contour features are tools used to derive and analyze shape statistics. For every contour pixel, a contour feature is determined, resulting in a vector as in (33).

$$fe = [fe_1, fe_2, ..., fe_n] \tag{33}$$

Opposite distance (dop): dop follows the normal line from the contour pixel p_i in the direction of the inner region, the first contour pixel $p_{op} = (x_{op}, y_{op})$ found, called its opposite pixel. The opposite distance is the Euclidean distance between a boundary pixel and its opposite pixel as in (34).

$$dop_i = \sqrt{(x_i - x_{op})^2 + (y_i - y_{op})^2} \tag{34}$$

Center of mass distance (dcm): Let $p_{cm} = (x_{cm}, y_{cm})$ is the coordinates of a shape's centroid. The Euclidean distance between the contour pixels $p_i = (x_i, y_i)$ and p_{cm}, is defined as the distance to the center of mass as in (35):

$$dcm_i = \sqrt{(x_i - x_{cm})^2 + (y_i - y_{cm})^2} \tag{35}$$

Distance between shapes: The distance between shapes P and Q is determined by means of a weighted sum of the distances relative to each contour features, as in (36):

$$d(P, Q) = w_{dcm} \times dcm(P, Q) + w_{op} \times dom(P, Q) \tag{36}$$

Where w_{op} and w_{dcm} are distinct weights for each feature. According to the respective feature vectors, $dop(P, Q)$ and $dcm(P, Q)$ are the distances between shapes P and Q, determined by (37) and (38):

$$dop(P, Q) = \sqrt{\sum_{i=1}^{q} (dop_{Pi} - dop_{Qi})^2} \tag{37}$$

and

$$dcm(P, Q) = \sqrt{\sum_{i=1}^{q} (dcm_{Pi} - dcm_{Qi})^2} \tag{38}$$

Where q is a number randomly selected to decrease feature vectors to a common perimeter, this is less than the perimeters of P and Q

2) Intensity Based Features (IBF) [46]:

IBF are mean, difference, standard deviation, skewness, and kurtosis.

The mean (μ) (39) is estimated to approximate the average intensity level in the ROI.

$$\mu = \frac{1}{N} \sum_{(p,q) \in ROI} I(p, q) \tag{39}$$

Where N is number of pixels in the ROI, The total

number of pixels in the ROI is I, and $I(p,q)$ is pixel intensity at (p,q).

The difference (40) between the lesion and surrounding normal liver tissue in mean gray level is:

$$difference(\mu) = \frac{1}{N}\sum_{(p,q)\in ROI} I_{Normal}(p,q) - \frac{1}{N}\sum_{(p,q)\in ROI} I_{Lesion}(p,q) \quad (40)$$

Where $I_{Normal}(p,q)$ pixel intensity at (p,q) of normal surrounding liver tissue ROI, and $I_{Lesion}(p,q)$ is pixel intensity at (p,q) of lesion ROI.

Standard deviation (σ) (41) is calculation of the distribution of intensity

$$\sigma = \sqrt{\sum_{h=0}^{L-1}(h-\bar{h})^2 P(h)} \quad (41)$$

Skewness (γ_1) (42) is symmetry estimation of histogram.

$$\gamma_1 = \frac{1}{\sigma^3}\sum_{h=0}^{L-1}(h-\bar{h})^3 * P(h) \quad (42)$$

Kurtosis (K) (43) is an estimate of the histogram tail.

$$K = \frac{\sum_{h=0}^{L-1}(h-\bar{h})^4}{(L-1)\sigma^4} \quad (43)$$

3) Texture Features (TF) [47]:

TF include gray level run length matrix (GLRLM), gray level co-occurance matrix (GLCM), and local binary pattern (LBP).

a) GLRLM [48]: A GLRLM is a matrix form of 2D histogram which measures the incidence of all various patterns of gray level values and gray level runs in an ROI for a given direction.

The run-length matrix $p(x,y)$ is the number of runs with pixels of gray level x and run length y. From this run-length matrix, various texture characteristics as given in (44)-(48) can then be extracted.

$$\text{Short Run Emphasis} = \frac{1}{n_r}\sum_{x=1}^{M}\sum_{y=1}^{N}\frac{p(x,y))}{y^2} \quad (44)$$

$$\text{Long Run Emphasis} = \frac{1}{n_r}\sum_{x=1}^{M}\sum_{y=1}^{N}p(x,y).y^2 \quad (45)$$

$$\text{Gray-Level Nonuniformity} = \frac{1}{n_r}\sum_{x=1}^{M}\left(\sum_{y=1}^{N}p(x,y)\right)^2 \quad (46)$$

$$\text{Run Length Nonuniformity} = \frac{1}{n_r}\sum_{y=1}^{N}\left(\sum_{x=1}^{M}p(x,y)\right)^2 \quad (47)$$

$$\text{Run Percentage} = \frac{n_r}{n_p} \quad (48)$$

b) GLCM [49]: GLCM is a matrix characterized as the distribution of co-occurring pixel values at a given offset over an image as given in (49)-(59).

$p(i,j)$ is (i,j)th element in a normalized gray tone spatial dependence matrix, $= \frac{P(i,j)}{R}$, $p_x(i)$ is ith element in the marginal probability matrix calculated by adding the rows of $p(i,j)$, $= \sum_{j=1}^{N_g} P(i,j)$, N_g is Number of dissimilar gray levels in the quantized image.

$$\text{Angular second moment(Energy)} = \sum_{i=1}^{N_g}\sum_{j=1}^{N_g}p(i,j)^2 \quad (49)$$

$$\text{Contrast} = \sum_{n=0}^{N_g-1}n^2\left\{\sum_{i=1}^{N_g}\sum_{j=1}^{N_g}p(i,j)\right\}, |i-j| = n \quad (50)$$

$$\text{Correlation} = \frac{\sum_{i=1}^{N_g}\sum_{j=1}^{N_g}(ij)p(i,j) - \mu_x\mu_y}{\sigma_x\sigma_y} \quad (51)$$

μ_x, μ_y σ_x, and σ_y are the means and standard deviations of p_x and p_y

$$\text{Sum of squares(variance)} = \sum_{i=1}^{N_g}\sum_{j=1}^{N_g}(1-\mu)^2 p(i,j) \quad (52)$$

$$\text{Inverse Differnce Moment} = \sum_{i=1}^{N_g}\sum_{j=1}^{N_g}\frac{1}{1+(i-j)^2}p(i,j) \quad (53)$$

$$\text{Sum Average} = \sum_{i=2}^{2N_g}(1-\text{Sum Entropy})^2\, p_{x+y}(i) \quad (54)$$

$$\text{Sum Entropy} = -\sum_{i=2}^{2N_g} p_{x+y}(i) log\left\{p_{x+y}(i)\right\} \quad (55)$$

$$\text{Entropy} = -\sum_{i=1}^{N_g}\sum_{j=1}^{N_g} p(i,j) log(p(i,j)) \quad (56)$$

$$\text{Difference Variance} = \text{variance of } p_{x-y} \quad (57)$$

$$\text{Difference Entropy} = -\sum_{i=0}^{N_g-1} p_{x-y}(i) log\left\{p_{x-y}(i)\right\} \quad (58)$$

$$\text{MCC} = (\text{second largest eigen value of } Q)^{\frac{1}{2}} \quad (59)$$

Where $Q(i,j) = \sum_{k=1}^{N_g} \frac{p(i,k)p(j,k)}{p_x(i)p_y(k)}$

c) Local binary pattern [50]: LBP is described as an order set of binary similarity of pixel intensities between the middle pixel and its 8-neighboring pixels. LBP do this evaluation by using (60):

$$LBP(x_c, y_c) = \sum_{n=0}^{7} s(i_n - i_c)2^n \quad (60)$$

Wherein i_c represent the center pixel value (x_c, y_c). LBP is applied to evaluate the local features in the image and also works by using fundamental LBP operator. Feature extracted matrix initially of 3×3, the elements are compared by the middle element, then binary pattern code is obtained and additionally LBP code is acquired by representing the binary code to decimal.

E. Feature Selection:

Feature selection is another common technique to decrease the number of characteristics in a data set. The distinction between the selection and the extraction of features is that the object of selecting features is to rank the value of existing features in the data set and discard secondary features. Optimization algorithms like PSO, genetic algorithm, ant colony optimization, sequential floating forward selection, sequential forward selection, simulated annealing, and dipolar decision tree are utilized to select the feasible features.

F. Classification [51]:

Methods widely used for classification include decision tree, support vector machine (SVM), neural network (NN), K-nearest neighbor (KNN) and bayes classifiers. Table IV discusses various methods used for LT classification. Comparison of various techniques by considering accuracy are discussed in Table V.

1) CNN

CNN is a particular form of multi-layer neural network as shown in Fig. 12 developed to identify visual patterns exactly from minimally pre-processed pixel images. The elements of CNN, like convolution and pooling layers, are substantially easy to interpret. The network learns to extract functions and the core idea is that it make use of image and filter convolution to produce invariant characteristics that are passed on to the next layer. In order to produce more invariant and descruptive features, the characteristics in the next layer are integrated with different filters and the process continues until the final feature that is invariant to occlusions is obtained. GoogLeNet, AlexNet, LeNet, ZFNet, ResNet, and VGGNet are the most widely used convolutional neural network architectures.

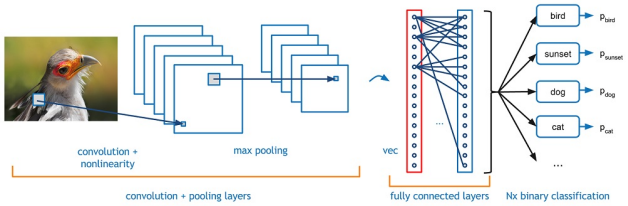

Figure 12. CNN

2) Artificial Neural Network (ANN):

ANN are statistical learning algorithms stimulated through the properties of biological NN and are applied for diverse responsibilities. As a system of interconnected computing elements, called nodes, ANNs are introduced that are operationally similar to biological neurons. The numerical values, called weights are assigned for the connections among distinctive nodes as shown in Fig. 13, and the network will ultimately approximate the favored characteristic with the aid of adjusting these values in a scientific way. As individual feature detectors, the hidden layers may be considered, detecting an increasing number of complicated styles within the information as it is propagated throughout the network. CNN, time delay neural network, radial basis function network, recurrent neural network, feed forward neural network, probabilistic neural network, and deep stacking network are the various forms of ANN.

3) SVM

The SVM is essentially a multidimensional space representation of distinct categories in a hyper plane. With the intention to reduce the error, the hyperplane may be inspired by way of the SVM in an iterative manner. The aim is to share the dataset into groups to obtain a greater marginal hyperplane as shown in Fig. 14. A great separation among the two classes is completed by the way of the hyperplane which has the maximum distance to the closest training data point in any class. The strength of algorithm relies on the kernel function. Linear kernels, gaussian kernels, and polynomial kernels are the most normally used kernels.

TABLE IV. COMPARISON OF LIVER TUMOR CLASSIFICATION TECHNIQUES

Ref	Images	Pre-processing	Liver segmentation	Tumor segmentation	Feature extraction	Feature selection	Classification	Validation
[52]	20 images from liveratlas database	Median filter	Thresholding technique and active contour	-	Segmentation based fractal textural analysis	-	SVM, Naive Bays Classifier	-
[53]	Private database	Median filter	Neutrosophic and FCM thresholding	-	GLCM	-	SVM	-
[54]	123 images from private hospitals	-	Adaptive thresholding	Spatial FCM	LBP, histogram, fourier based features	-	Multilayer perceptron and C4.5 Decision tree	k-fold validation
[55]	20 CT from 3DIRCADS, 100 CT from private database	-	Region growing	Kernelized FCM	Intensity and texture based features from liver and tumor	Variation of features obtained from liver and tumor	SVM	-
[56]	200 Fused images (MRI&CT)	Gabor filter	Otsu thresholding	-	254 hybrid features	Probability of error plus average correlation	Multilayer perceptron, SVM, Random forest J48	10 fold cross validation
[6]	LiTS dataset and private dataset	HE, MF	Adaptive thresholding and level set segmentation	Fuzzy centroid based region growing algorithm	GLCM, shape features, and LBP	-	RNN and CNN with O-SHO	

4) KNN

KNN is a non-parametric approach employed for classification and regression. The input in both instances comprise of the k nearest training examples in the space of the function. In KNN, the features are best locally estimated and all calculations are delayed before assessment of the feature. A distance metric or similarity feature is specified, in which the common alternatives encompass the euclidean distance and manhattans distance, with the intention to follow the KNN classification. Result is a membership of the class. An object is described via its neighbor's plurality of votes, with the object being allocated to the class most similar among its nearest neighbors. If $k = 1$, then the object is certainly allotted to the nearest neighbor's class.

5) Random Forest Algorithm (RFA)

A supervised learning algorithm which is applied for classification and regression is RFA. As we understand that a forest is made from bushes and more trees implies more durable forest, in addition, RFA generates decision trees on data samples and then gets prediction of each them and ultimately chooses the high-quality solution by voting. It is a collaborative approach that is higher than a single selection tree because with the aid of combining the result, it decreases the over-fitting. The RFA is a set of rules for category inclusive of numerous choice bushes. When constructing each character tree, it makes use of bagging and feature randomness to try to construct an uncorrelated forest of trees whose prediction by way of committee is more unique than that of any individual tree as shown in Fig. 15.

G. Validation [57]:

Cross Validation (CV) is a method involving the reservation of a sample of a dataset on which the model is not trained. Later, before finalizing the model, it will be tested using this dataset. Here are the steps that cross validation involves:

TABLE V. COMPARISON OF PERFORMANCE OF VARIOUS TECHNIQUES

Ref	Features	Classifier	Optimization algorithm	Feature reduction	Modality and organ	Accuracy
[60]	34 features "textural, color, shape"	deep belief network (DBN)	grasshopper	Principal Component Analysis (PCA)	CT Liver	98%
[61]	72 multi-level fractal features, 132 multi-domain features	Six multi-class ensemble classifiers namely AdaBoostM2, Bag, LPBoost, RUSBoost, Subspace, and TotalBoost	PSO	ReliefF	Ultrasound Liver	91%
[62]	GLCM	ANN	-	opposition fruit fly	MRI and CT Liver	97.5%
[63]	Mean, Variance, Skewness and Kurtosis	Similarity Search based Hybrid Classification distance technique	-	-	CT Liver	93%
[64]	GLCM and DWT method	KSVM	-	PCA	MRI Brain	97%

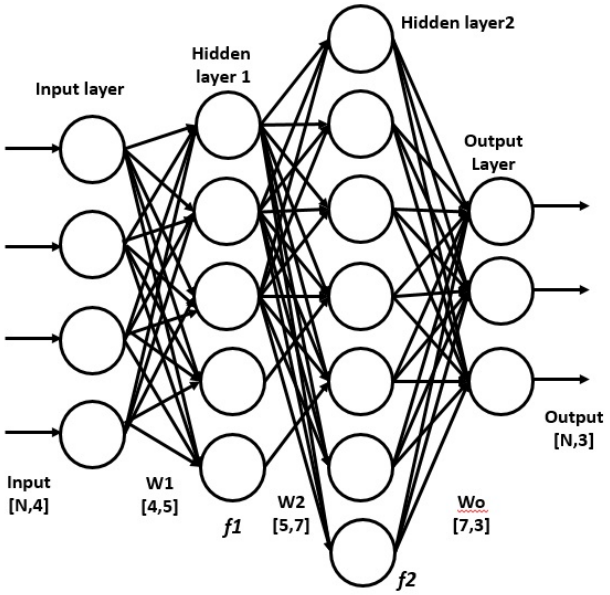

Figure 13. ANN

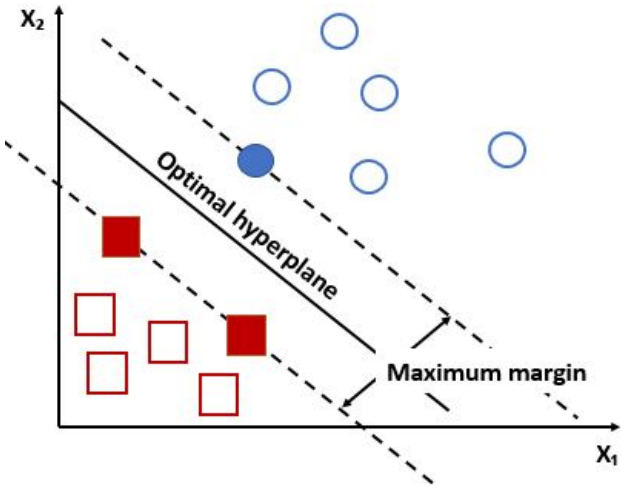

Figure 14. SVM

- Reserve a sample data
- Use the remaining data to train the model
- Use the reserve sample data to the test (validation).

In order to break the data into three sections, namely, train, validation and test sets, a simple approach is followed. But this approach normally does not perform well in situations where large datasets is not available. The dataset is divided into train and validation sets, which may cause few data points with valuable information to be omitted from the training procedure when there is limited information, and the model is unable to understand the distribution of data.

Compared to other models, the K-fold CV offers a paradigm with less bias. The dataset is allotted to number of folds specified by parameter K in the K-fold CV as shown in Fig. 16. This parameter specifies how many folds the dataset will be split into. In the training set $(K-1)$ times,

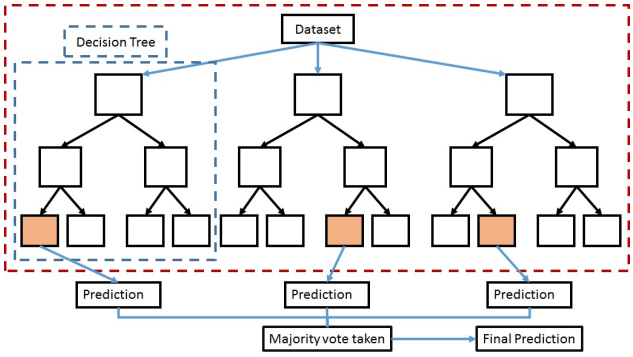

Figure 15. Random Forest Algorithm

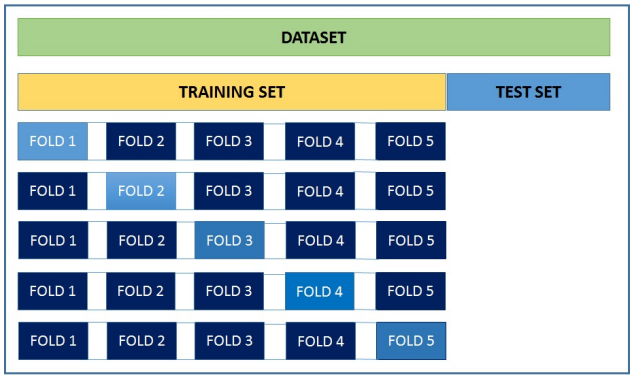

Figure 16. K-Fold Cross Validation

every fold is likely to appear, which in turn means that every observation in the dataset emerges in the dataset, allowing the model to better understand the basic distribution of data.

The value used for $'K'$ normally varies from 5 to 10. A highly biased model is obtained if K value is too low (say $K = 2$). This situation is comparable to the division of the dataset into training and validation sets, so the bias would be high and the low variance. If the K is high, this method is called Leave One Out CV.

4. Discussion and Scope of Research

Each day, the majority of individuals with liver issues increase, which is owing to the tremendous quantity of CT images to be examined, the oncologists have been overloaded. The integration of CAD systems as a useful resource tool for clinicians is therefore important. The systems designed until now, but, have inherent drawbacks which must be resolved to make them effective in a health-care context.

In traditional CAD structures, extensive research has been carried out thoroughly to investigate automate the method of segmentation. The structure and presence of liver and liver tumors, however, are likely to vary, so the development of a fully automatic segmentation algorithm is not realistic. Methods for segmentation should be built which can simultaneously remove segmentation errors.

As the amount of CT data analyzed by the CAD system is indeed huge, a further significant issue would be to concentrate on establishing easier and computer-efficient algorithms. The lesions may be identified explicitly from the CT images rather than the hierarchical approach, to minimize complexity to a certain degree.

Another critical problem in the CAD system is the selection of the required features that correctly describe the various groups of liver lesions. Various specialists have researched the adequacy of different high-quality features. The most distinguishing characteristics of the particular lesions, however, have not been found till now

An area that must be emphasized is that a huge public database should be established devoted to liver cancers. There are minimal published CT images on the current public datasets. Therefore, in much of the literature reviewed, private hospital datasets have been used. Consequently, comparing the overall quality of CAD systems is challenging.

5. Proposed Method

Initially, images are preprocessed, then LS is done by using conventional methods. Next, an enhanced deep learning method is used for LT segmentation, then features such as "GRLM, shape features, GLCM, local ternary pattern, and LBP" will be extracted from the tumor. Finally, the hyperparameter tuned-deep neural network is used for classification. This method may give high accuracy compared to other methods.

6. Conclusion

This paper explores the different methods utilized for the segmentation and classification of liver anomalies identified in traditional and DL-based CAD systems. The techniques utilized for the segmentation of liver lesions are also mentioned. A CAD structure helps to assist a specialist in the decision-making step by correctly identifying the anomalies and thus giving a subsequent decision. CAD structures could recognize the tumors that a radiologist might miss to be of practical benefit. Although a great deal of exploration has been carried out over the most recent twenty years, there is indeed space for further research as it is important to build powerful CAD systems that offer fully automatic identification of liver tumors, less complicated and accurate for medical care.

Abrevations

ACM, Active Contour Model; ACS, American Cancer Society; ADF, Anisotropic Diffusion Filter; AFP, Alpha-Fetoprotein; AMBE, Absolute Mean Brightness Error; ANN, Artificial Neural Network; ANOVA, Analysis of Variance; ASD, Average Symmetric Distance; BF, Bilateral Filter; BLT , Benign Liver Tumor; BM3D, Block-Matching and 3D Filtering; CNN, Convolutional Neural Network; cSE, channel Excitation; CT, Computed Tomography; CV, Cross Validation; dcm, Center of mass distance ; DICE,

Dice similarity coefficient; DL, Deep Learning; dop, Opposite distance; DWT, Discrete Wavelet Transform; ED, Entropy Difference; EL, Ensemble Learning; FCM, Fuzzy C-Means; FCN, Fully Convolutional Network; FE, Feature Extraction; FFCM, Fast Fuzzy C-Means; FNH, Focal Nodular Hyperplasia; GCM, Graph-Cut Method; GF, Gaussian Filter; GLCM, Gray Level Co-occurrence Matrix; GLRLM, Gray Level Run Length Matrix; HA, Hepatic Adenoma; HCC, Hepatocellular Carcinoma; HE, Histrogram Equalisation; IBDC, Intrahepatic Bile Duct Cancer; IBF, Intensity Based Features; IoU, Intersection over Union; IP, Image Processing; IQI, Image Quality Index; KNN, K-Nearest Neighbor; LBP, Local Binary Pattern; LC, Liver Cancer; LT, Liver Tumor; LS, Liver Segmentation; KSVM, Kernel based Support Vector Machine; MaxD, Maximum symmetric surface Distance; MCC, Maximum Correlation Coefficient; MF, Median Filter; MI, Mutual Information; MRI, Magnetic Resonance Imaging; MSE, Mean Square Error; NLM, Non-Local Means; NS, Neutrosophic Set; NSCT, Non-Subsampled Contourlet Transform; O-SHO, Opposition-based Spotted Hyena Optimization; PLC, Primary Liver Cancer; PSO, Particle Swarm Optimization; PCA, Principle Component Analysis; QRCM, Quality-aware Relative Contrast Measure; RBS, Region-Based Segmentation; ResNet, Residual neural Network; RFA, Random Forest Algorithm; RMSD, Root Mean Square symmetric surface Distance; RMSE, Root Mean Square Error; RVD, Relative Volume Difference; RN, Residual Network; RNN, Recurrent Neural Network; SLC, Secondary Liver Cancer; SSC, Sparse shape component; SSIM, Structural Similarity Index Measure; STD, Standard Deviation; SVD, Singular Value Decomposition; SVM, Support Vector Machine; TF, Texture Features; TNM, tumor (T), nodes (N), and metastases (M); TPR, True Positive Rate; UIQI, Universal Image Quality Index; US, United States; VOE, Volumetric Overlap Error; WF, Wiener Filter; WPSNR, Weighted Peak Signal to Noise Ratio.

References

[1] https://www.ohsu.edu/knight-cancer-institute/understanding-liver-cancer

[2] https://www.biospace.com/article/insight-report-liver-cancer/

[3] https://www.cancer.org/cancer/liver-cancer/detection-diagnosis-staging.html

[4] Megha Ganjre, J. P. Gawande, "Automated Segmentation Of Liver And Tumour And Feature Extraction From Abdominal Ct Images Using Region Growing Method", International Journal of Advances in Science Engineering and Technology, ISSN: 2321-9009 Volume-2, Issue-4, Oct.-2014, pp. 30-35

[5] Dirk Smeets, Dirk Loeckx, Bert Stijnen, Bart De Dobbelaer, Dirk Vandermeulen, Paul Suetens, "Semi-automatic level set segmentation of liver tumors combining a spiral-scanning technique with supervised fuzzy pixel classification", Medical Image Analysis, Volume 14, Issue 1, 2010, Pages 13-20, ISSN 1361-8415, doi: 10.1016/j.media.2009.09.002.

[6] Munipraveena Rela, Suryakari Nagaraja Rao, Patil Ramana Reddy, "Optimized segmentation and classification for liver tumor Segmentation and classification using opposition-based spotted hyena optimization", International Journal of Imaging Systems and Technology, 2020, 1–30, DOI: 10.1002/ima.22519.

[7] Yuan Y, Chen YW, Dong C, Yu H, Zhu Z. Hybrid method combining superpixel, random walk and active contour model for fast and accurate liver segmentation. Computerized Medical Imaging and Graphics, 2018 Dec; 70 pp. 119-134. doi: 10.1016/j.compmedimag.2018.08.012

[8] Yang Li, Yu-qian Zhao, Fan Zhang, Miao Liao, Ling-li Yu, Baifan Chen, Yan-jin Wang, Liver segmentation from abdominal CT volumes based on level set and sparse shape composition, Computer Methods and Programs in Biomedicine, Volume 195, 2020, 105533, ISSN 0169-2607, doi: 10.1016/j.cmpb.2020.105533.

[9] Abdul Qayyum, Alain Lalande, Fabrice Meriaudeau, Automatic segmentation of tumors and affected organs in the abdomen using a 3D hybrid model for computed tomography imaging, Computers in Biology and Medicine, Volume 127, 2020, 104097, ISSN 0010-4825, doi: 10.1016/j.compbiomed.2020.104097.

[10] Ahmed M. Anter, Aboul Ella Hassenian, Computational intelligence optimization approach based on particle swarm optimizer and neutrosophic set for abdominal CT liver tumor segmentation, Journal of Computational Science, Volume 25, 2018, Pages 376-387, ISSN 1877-7503, doi: 10.1016/j.jocs.2018.01.003.

[11] Ahmed M. Anter, Aboul Ella Hassenian, CT liver tumor segmentation hybrid approach using neutrosophic sets, fast fuzzy c-means and adaptive watershed algorithm, Artificial Intelligence in Medicine, Volume 97, 2019, Pages 105-117, ISSN 0933-3657, doi: 10.1016/j.artmed.2018.11.007.

[12] A. Baazaoui, W. Barhoumi, A. Ahmed, E. Zagrouba, Semi-Automated Segmentation of Single and Multiple Tumors in Liver CT Images Using Entropy-Based Fuzzy Region Growing, IRBM,Volume 38, Issue 2, 2017, Pages 98-108, ISSN 1959-0318, doi: 10.1016/j.irbm.2017.02.003.

[13] Lei Xu, Yingliang Zhu, Yuhao Zhang, Haima Yang, Liver segmentation based on region growing and level set active contour model with new signed pressure force function, Optik, Volume 202, 2020, 163705, ISSN 0030-4026, doi: 10.1016/j.ijleo.2019.163705.

[14] X. Zhang, J. Tian, D. Xiang, X. Li and K. Deng, "Interactive liver tumor segmentation from ct scans using support vector classification with watershed," 2011 Annual International Conference of the IEEE Engineering in Medicine and Biology Society, Boston, MA, 2011, pp. 6005-6008, doi: 10.1109/IEMBS.2011.6091484.

[15] Munipraveena Rela, Suryakari Nagaraja Rao and Patil Ramana Reddy, "Liver Tumor Segmentation using Superpixel based Fast Fuzzy C Means Clustering" International Journal of Advanced Computer Science and Applications, 11(11), 2020. DOI:10.14569/IJACSA.2020.0111149

[16] Abhijeet Patil, Prof. Mrs. V. S. Kulkarni, "A Review: Liver Cancer Detection Algorithm", International Journal of Advanced Research in Computer and Communication Engineering Vol. 5, Issue 6, June 2016, DOI: 10.17148/IJARCCE.2016.56194 859

[17] Mehrdad Moghbel, Syamsiah Mashohor, Rozi Mahmud, M. Iqbal Bin Saripan, "Review of liver segmentation and computer assisted detection/diagnosis methods in computed tomography", Artificial Intelligence Review volume 50, pages497–537(2018). doi:10.1007/s10462-017-9550-x

[18] S. Priyadarsini and D. Selvathi, "Survey on segmentation of liver from CT images," 2012 IEEE International Conference on Advanced Communication Control and Computing Technologies (ICACCCT), Ramanathapuram, 2012, pp. 234-238, doi: 10.1109/ICACCCT.2012.6320777.

[19] Manoj Diwakar, Manoj Kumar, "A review on CT image noise and its denoising", Biomedical Signal Processing and Control, Volume 42, 2018, Pages 73-88, ISSN 1746-8094, doi: 10.1016/j.bspc.2018.01.010.

[20] M. Rela, N. R. Suryakari and P. R. Reddy, "Liver Tumor Segmentation and Classification: A Systematic Review," 2020 IEEE-HYDCON, Hyderabad, India, 2020, pp. 1-6, doi: 10.1109/HYDCON48903.2020.9242757

[21] Munipraveena Rela, "CT Liver Image Enhancement using Spatial Filters", International Journal of Innovative Technology and Exploring Engineering (IJITEE) ISSN: 2278-3075, Vol. 8, Issue-11S2, September 2019, pp. 30-32, DOI: 10.35940/ijitee.K1005.09811S219.

[22] Munipraveena Rela, S. Nagaraja Rao, P. Ramana Reddy, "Efficient Image Enhancement Techniques Applied on Medical Imaging-A State- of- The Art Survey", International Journal of Recent Technology and Engineering, ISSN: 2277-3878, Vol. 7, Issue-6S4, April 2019, pp. 285-289.

[23] Zohair Al-Ameen, Ghazali Sulong and Md. Gapar Md. Johar, "Enhancing the Contrast of CT Medical Images by Employing a Novel Image Size Dependent Normalization Technique", International Journal of Bio-Science and Bio-Technology, Vol. 4, No. 3, pp. 63-68, Sep. 2002.

[24] Fathi KALLEL, Ahmed BEN HAMIDA, "A new adaptive gamma correction based algorithm using DWT-SVD for non-contrast CT image enhancement", IEEE Transactions on NanoBioscience Vol. 16 , Issue: 8 , pp. 666 - 675, Dec. 2017.

[25] P. Sreeja, S. Hariharan, "An improved feature based image fusion technique for enhancement of liver lesions" Biocybernetics and Biomedical Engineering Volume 38, Issue 3, pp. 611-623, May 2018.

[26] Manoj Diwakar, Manoj Kumar, "CT image denoising using NLM and correlation-based wavelet packet thresholding", IET Image Processing, Vol. 12 Iss. 5, pp. 708-715, 2018.

[27] Das K., Maitra M., Sharma P., Banerjee M. (2019) Early Started Hybrid Denoising Technique for Medical Images. In: Bhattacharyya S., Mukherjee A., Bhaumik H., Das S., Yoshida K. (eds) Recent Trends in Signal and Image Processing. Advances in Intelligent Systems and Computing, vol 727. Springer, Singapore.

[28] Huafeng Li, Xiaoge He, Dapeng Tao, Yuanyan Tang, Ruxin Wang, "Joint medical image fusion, denoising and enhancement via discriminative low-rank sparse dictionaries learning" Pattern Recognition, vol. 79, pp. 130–146, Feb. 2018.

[29] Jinlan Guan, Jiequan Ou, Zhihui Lai and Yuting Lai, "Medical Image Enhancement Method Based on the Fractional Order Derivative and the Directional Derivative", International Journal of Pattern Recognition and Artificial Intelligence, Vol. 32, No. 3, pp. 1857001 (22 pages), 2018.

[30] Ebenezer Daniel,J.Anitha, "Optimum wavelet based masking for the contrast enhancement of medical images using enhanced cuckoo search algorithm", Computers in Biology and Medicine, Volume 71, Pages 149-155, April 2016.

[31] X. Zheng, S. Ravishankar, Y. Long and J. A. Fessler, "PWLS-ULTRA: An Efficient Clustering and Learning-Based Approach for Low-Dose 3D CT Image Reconstruction," in IEEE Transactions on Medical Imaging, vol. 37, no. 6, pp. 1498-1510, June 2018

[32] Suhuai Luo, Xuechen Li, Jiaming Li, "Review on the Methods of Automatic Liver Segmentation from Abdominal Images", Journal of Computer and Communications, 2014, 2, 1-7, doi: 10.4236/jcc.2014.22001

[33] S. Morfu, "Image processing using diffusion processes," Proceedings of 2010 IEEE International Symposium on Circuits and Systems, Paris, 2010, pp. 1811-1814, doi: 10.1109/ISCAS.2010.5537719.

[34] R.J. Hemalatha, T.R. Thamizhvani, A. Josephin Arockia Dhivya, Josline Elsa Joseph, Bincy Babu and R. Chandrasekaran (July 4th 2018). Active Contour Based Segmentation Techniques for Medical Image Analysis, Medical and Biological Image Analysis, Robert Koprowski, IntechOpen, DOI: 10.5772/intechopen.74576

[35] I. Cruz-Aceves, J. G. Avina-Cervantes, J. M. Lopez-Hernandez, M. G. Garcia-Hernandez, M. Torres-Cisneros, H. J. Estrada-Garcia, and A. Hernandez-Aguirre, "Automatic Image Segmentation Using Active Contours with Univariate Marginal Distribution", Hindawi Publishing Corporation, Mathematical Problems in Engineering, Volume 2013, Article ID 419018, 9 pages, doi: 10.1155/2013/419018

[36] Salem Saleh Al-amri, N.V. Kalyankar and Khamitkar S.D, "Image Segmentation by Using Threshold Techniques", JOURNAL OF COMPUTING, VOLUME 2, ISSUE 5, MAY 2010, ISSN 2151-9617

[37] https://missinglink.ai/guides/computer-vision/image-segmentation-deep-learning-methods-applications/

[38] T.H. Le, S.-W. Jung, K.-S. Choi and S.-J. Ko, "Image segmentation based on modified graph-cut algorithm", ELECTRONICS LETTERS, 5th August 2010, Vol. 46, No. 16, p. 1121 – 1123, DOI: 10.1049/el.2010.1692

[39] Tara Saikumar, P. Yugander, P. S. Murthy, and B. Smitha, "Image Segmentation Algorithm Using Watershed Transform and Fuzzy C-Means Clustering on Level Set Method", International Journal of Computer Theory and Engineering, Vol. 5, No. 2, April 2013, 209-213. 10.7763/IJCTE.2013.V5.680.

[40] Almotairi, S., Kareem, G., Aouf, M., Almutairi, B., and Salem, M. A. (2020). Liver Tumor Segmentation in CT Scans Using Modified SegNet. Sensors (Basel, Switzerland), 20(5), 1516. DOI: 10.3390/s20051516

[41] Huiyan Jiang, Shaojie Li, and Siqi Li, "Registration-Based Organ Positioning and Joint Segmentation Method for Liver and Tumor Segmentation", Hindawi, BioMed Research International, Volume 2018, Article ID 8536854, 11 pages, DOI: 10.1155/2018/8536854, Sep 2018.

[42] Weiwei Wu, Shuicai Wu, Zhuhuang Zhou, Rui Zhang, and Yanhua Zhang, "3D Liver Tumor Segmentation in CT Images Using Improved Fuzzy C-Means and Graph Cuts", Hindawi, BioMed Research International, Volume 2017, Article ID 5207685, 11 pages, DOI: 10.1155/2017/5207685, Sep 2017.

[43] A. I. Poernama, I. Soesanti and O. Wahyunggoro, "Feature Extraction and Feature Selection Methods in Classification of Brain MRI Images: A Review," 2019 International Biomedical Instrumentation and Technology Conference (IBITeC), Special Region of Yogyakarta, Indonesia, 2019, pp. 58-63, doi: 10.1109/IBITeC46597.2019.9091724

[44] Yang Mingqiang, Kpalma Kidiyo and Ronsin Joseph, "A Survey of Shape Feature Extraction Techniques" Pattern Reconginition Techniques, Technology and Applications, Book edited by: Peng-Yeng Yin, ISBN 978-953-7619-24-4, pp. 626, November 2008, I-Tech, Vienna, Austria.

[45] J. C. Figueiredo, F. G. Medeiros Neto and I. C. de Paula, "Contour-based feature extraction for image classification and retrieval," 2016 35th International Conference of the Chilean Computer Science Society, Valparaiso, 2016, pp. 1-7, doi: 10.1109/SCCC.2016.7836058.

[46] K. D. Kharat, V. J. Pawar and S. R. Pardeshi, "Feature extraction and selection from MRI images for the brain tumor classification," 2016 International Conference on Communication and Electronics Systems, Coimbatore, 2016, pp. 1-5, doi: 10.1109/CESYS.2016.7889969.

[47] W. Kuo, "Computer-aided diagnosis for feature selection and classification of liver tumors in computed tomography images," 2018 IEEE International Conference on Applied System Invention, 2018, pp. 1207-1210, doi: 10.1109/ICASI.2018.8394505

[48] Xiaoou Tang, "Texture information in run-length matrices," in IEEE Transactions on Image Processing, vol. 7, no. 11, pp. 1602-1609, Nov. 1998, doi: 10.1109/83.725367

[49] R. M. Haralick, K. Shanmugam and I. Dinstein, "Textural Features for Image Classification," in IEEE Transactions on Systems, Man, and Cybernetics, vol. SMC-3, no. 6, pp. 610-621, Nov. 1973, doi: 10.1109/TSMC.1973.4309314.

[50] Md. Abdur Rahim, Md. Najmul Hossain, Tanzillah Wahid, and Md. Shafiul Azam, "Face Recognition using Local Binary Patterns (LBP)", Global Journal of Computer Science and Technology Graphics and Vision, Volume 13 Issue 4 Version 1.0 Year 2013, Online ISSN: 0975-4172

[51] https://medium.com/analytics-vidhya/image-classification-techniques-83fd87011cac

[52] 1. A. Krishna, D. Edwin and S. Hariharan, "Classification of liver tumor using SFTA based Naïve Bayes classifier and support vector machine," 2017 International Conference on Intelligent Computing, Instrumentation and Control Technologies, 2017, pp. 1066-1070, doi: 10.1109/ICICICT1.2017.8342716.

[53] Muthuswamy J. (2019) Extraction and Classification of Liver Abnormality Based on Neutrosophic and SVM Classifier. Progress in Advanced Computing and Intelligent Engineering. Advances in Intelligent Systems and Computing, vol 713. doi:10.1007/978-981-13-1708-8-25

[54] Amita Das, Priti Das, S. S. Panda, and Sukanta Sabut, Detection of Liver Cancer Using Modified Fuzzy Clustering and Decision Tree Classifier in CT Images. Pattern Recognition and Image Analysis, 2019, Vol. 29, No. 2, pp. 201–211. doi:10.1134/S1054661819020056

[55] Devi, R.M., Seenivasagam, V. Automatic segmentation and classification of liver tumor from CT image using feature difference and SVM based classifier-soft computing technique. Soft Comput 24, 18591–18598 (2020). doi:10.1007/s00500-020-05094-1

[56] Naeem S, Ali A, Qadri S, Khan Mashwani W, Tairan N, Shah H, Fayaz M, Jamal F, Chesneau C, Anam S. Machine-Learning Based Hybrid-Feature Analysis for Liver Cancer Classification Using Fused (MR and CT) Images. Applied Sciences. 2020; 10(9):3134. DOI:10.3390/app10093134

[57] https://medium.com/the-owl/k-fold-cross-validation-in-keras-3ec4a3a00538

[58] Shenhai Zheng, Bin Fang, Laquan Li, Mingqi Gao, Yi Wang, and Kaiyi Peng (2020) Automatic liver tumour segmentation in CT combining FCN and NMF-based deformable model, Computer Methods in Biomechanics and Biomedical Engineering: Imaging and Visualization, 8:5, 468-477, DOI: 10.1080/21681163.2018.1493618

[59] Z. Bai, H. Jiang, S. Li and Y. Yao, "Liver Tumor Segmentation Based on Multi-Scale Candidate Generation and Fractal Residual Network," in IEEE Access, vol. 7, pp. 82122-82133, 2019, doi: 10.1109/ACCESS.2019.2923218.

[60] Renukadevi, T, Karunakaran, S. Optimizing deep belief network parameters using grasshopper algorithm for liver disease classification. Int J Imaging Syst Technol. 2020; 30: 168– 184. DOI: 10.1002/ima.22375

[61] Krishnamurthy, RK, Radhakrishnan, S, Kattuva, MAK. Particle swarm optimization[U+2010]based liver disorder ultrasound image classification using multi[U+2010]level and multi[U+2010]domain features. Int J Imaging Syst Technol. 2020; 1– 20. DOI:10.1002/ima.22518

[62] Krishan, Abhay and Mittal, Deepti. "Effective segmentation and classification of tumor on liver MRI and CT images using multi-kernel K-means clustering" Biomedical Engineering / Biomedizinische Technik, vol. 65, no. 3, 2020, pp. 301-313. DOI:10.1515/bmt-2018-0175

[63] Sakthisaravanan, B., Meenakshi, R. OPBS-SSHC: outline preservation based segmentation and search based hybrid classification techniques for liver tumor detection. Multimed Tools Appl 79, 22497–22523 (2020). DOI:10.1007/s11042-019-08582-1

[64] Pareek M., Jha C.K., Mukherjee S. (2020) Brain Tumor Classification from MRI Images and Calculation of Tumor Area. Soft Computing: Theories and Applications. Advances in Intelligent Systems and Computing, vol 1053. Springer.

Munipraveena Rela Munipraveena Rela received M.Tech in Electronics from BMS College of Engineering in the year 2005. Currently she is pursuing Ph.D. from JNTUA, Ananthapur in the area of medical image analysis. She has published 21 research papers in various National and International Journals/Conferences. Her research includes image processing, signal processing and VLSI.

Dr. S. Nagaraja Rao Dr. S. Nagaraja Rao received M. Tech in Digital Systems and Computer Electronics from J.N.T.University, Hyderabad in 1998 and Ph.D. in the area of Signal and Image Processing from Jawaharlal Nehru Technological University Ananthapuramu (JNTUA) in 2011. Presently he is working as Professor and Head, Department of ECE, G. Pulla Reddy Engineering College (Autonomous), Kurnool, AP, India. He has 30 years of experience from this 7years in the Industry and 23 Years in Teaching. His research interest includes signal processing, Image Processing and VLSI. He has more than 50 research publications in various International/National Journals/Conferences. He is currently guiding 7 PhD scholars. He is Life member of ISTE, Life member of Instrument Society of India (ISOI), member of IEEE.

Dr. P Ramana Reddy Dr. P Ramana Reddy received the M.E (Electronics) from SGGSCET, Nanded, Maharashtra in 1994 and Ph.D. in the area of Image Processing from Jawaharlal Nehru Technological University Ananthapuramu (JNTUA) in 2010. Presently he is working as Professor, Department of ECE, JNTUA College of Engineering, Ananthapuramu, AP, and India. He has 25 years of teaching and 17 years of research experience. His research interest includes signal processing, Image Processing, VLSI, and wireless communication. He has about 125 research publications in various International/National Journals/Conferences. He is currently guiding 15 and guided 8 PhD students. He is fellow of IEI and IETE and life member of ISTE.